J Nanostruct 9(4): 650-658, Autumn 2019

RESEARCH PAPER

Sol-Gel Synthesis and Piezoelectric and Structural Properties of Zr –rich PZT Nanoparticles

Seyed Mohammad Taheri Otaqsara[1], Ali Azam Khosravi 1, Reza Tabarzadi[2]*

[1] *Department of Physics, Shahed University, Tehran, Iran*

[2] *Materials and Energy Research Center, Meshkinshahr, Karaj, Iran*

ARTICLE INFO

Article History:
Received 21 May 2019
Accepted 08 July 2019
Published 01 October 2019

Keywords:
Electromechanical Coupling Factor
Nanopowder
Perovskite
Piezoelectric
PZT Nanostructure

ABSTRACT

Lead zirconate titanate (PZT) nanopowders with spherical-shaped morphology, perovskite structure and an average size of 20 nm were successfully synthesized. The prepared PZT nanopowders were characterized by differential thermal analysis (DTA), X-ray diffraction (XRD), scanning electron microscopy (SEM), Energy dispersive X-ray (EDS) and Transmission electron microscopy (TEM) technique. Single-phase perovskite PZT nanopowders were obtained after heat treatment at temperature of 700 °C. The effect of calcination temperature on crystal structure of PZT nanopowders has been discussed. Dielectric relaxation of the ferroelectric ceramics could originate from the alternations of the elastic and electric behavior and the movement of the domain walls at high frequency regions. To determine piezoelectric property of ceramics, resonant vibration spectrum of samples was measured at room temperature. A relative density of 7.53 g/cm3 was achieved at sintering temperature of 1150 °C, which is close to the theoretical density (~95%). At higher temperature sint, the density of ceramic samples strongly decreases which can be attributed to the evaporation of excess PbO. The optimum values of piezoelectric constant, electromechanical quality factor and a mechanical quality factor are obtained at Sintering temperature 1150 °C: d_{33}=64 pC/N, K_p=0.41 and Q_m=34.3.

How to cite this article
Taheri Otaqsara SM, Azam Khosravi A, Tabarzadi R. Sol-Gel Synthesis and Piezoelectric and Structural Properties of Zr –rich PZT Nanoparticles. J Nanostruct, 2019; 9(4): 650-658. DOI: 10.22052/JNS.2019.04.007

INTRODUCTION

Pb-based perovskite solid solution of lead zirconate titanates (PZT; $Pb(Zr_xTi_{1-x})O_3$) have been considered due to its high spontaneous polarization abilities, piezoelectric coefficient, dielectric permittivity and pyroelectricity [1,2]. The highest values for piezoelectric coefficient (d_{33}) and the permittivity (ε_r) have been observed for chemical composition of x=0.52, the so-called morphotropic phase boundary (MPB), at which the tetragonal (Ti-rich) and rhombohedral (Zr-rich) phases coexist [3,4]. The excellent piezoelectric properties make it a promising material for sensors, optoelectronic and electromechanical transducer application [5]. Nano-sized particles of ferroelectric materials exhibited significant properties which recently motivated many in-depth researches on future applications [6-8]. For example, PZT nanoparticles (PZT-NPs) can also be suspended in PZT sol to serve as seeds to lower sintering temperature and reduction of Pb loss [9].

Currently, there are two approaches to make PZT-NPs. The first way is a top-down approach often used in the industry [10]. The second method is a bottom-up approach that is still underactive investigation by various researchers. Size and quality of PZT-NPs are controlled by various process parameters, such as temperature, time, and mineralizer concentration [11-15]. A wide variety of preparation routes have been employed to produce PZT-NPs such as hydrothermal [16,17], electrodynamics atomization [18,19], ultrasonic

* *Corresponding Author Email: mohammad.taheri2712@yahoo.com*

spray combustion synthesis (USCs) [20] and sol-gel [21-23]. Among these techniques, sol-gel process provides the advantage of homogenous chemistry in multi-component system, ease of composition variation, and low processing temperature [24]. Acetic acid based sol–gel processing of PZT, introduced by Yi *et al*. [25], and later developed by Assink and Schwartz [26], offers a simpler preparation route compared to the 2-methoxyethanol based sol–gel. The method was based on the reduced reactivity of transition metal alkoxides by acetic-acid modification.

In the present study, PZT precursor solution was prepared from different metal-organic compounds and different experimental processes. Then, PZT nanopowders were synthesized by acid acetic based sol-gel method. The properties of PZT nanopowders were investigated to evaluate the effect of calcination temperature on the crystal structure of PZT nanopowders by using an X-ray diffractometer (XRD). The electromechanical and piezoelectric behavior of PZT was determined by the resonance/anti-resonance method.

MAERIALS AND METHODS

The chemicals used to prepare the PZT sol were; lead acetate trihydrate ($Pb(C_2H_3O_2)_2$. $3H_2O$, denoted as $Pb(OAc)_2$. $3H_2O$, Merck.), tetra-iso-propylitanate (aka titanium-isopropoxide, $Ti[OCH(CH_3)_2]_4$, denoted as $Ti(O^ipr)_4$, Sigma-Aldrich Co.), zirconium n-propoxide solution with 70% $^{w/w}$ in n-propanol ($Zr[O(CH_2)_2CH_3]_4$, denoted as $Zr(Opr)_4$, Sigma-Aldrich Co.), glacial acetic acid (HOAc, Sigma-Aldrich Co., 99.7% pure) and acetylacetone ($C_5H_8O_2$, denoted as AcAc, Merck Co.).

Synthesis

First, 13.9 gr $Pb(OAc)_2.3H_2O$ was dissolved in acetic acid on a 1:3 molar ratio while stirred and refluxed at 110 °C during 3 h for dehydration and homogeneity purposes (solution A). Subsequently, 0.48 gr Ti $(O^ipr)_4$ was mixed with (2.52 gr) acetylacetone in order to avoid fast hydrolysis of reactants and continuously stirred at room temperature for 4h. Then 14.8 gr $Zr(Opr)_4$ was t added into the mixture, which will be referred hereafter as solution B. Pb and Zr/Ti precursor solutions were then mixed and refluxed for 3 h at 85 °C. For hydrolysis, 1.8 gr of distilled water was added to it and pH value was adjusted using Hydrochloride acid to allow the nanoparticle precursor to slow grow. The solution was stirred overnight at room temperature to get slightly yellowish clear transparent sol and then heated at 70 °C to obtain the gelation of Zr -rich PZT sol. The gel was dried at 120 °C and heat treated in two stages. The first heat treatment was carried out at 400 °C/ 2h with a heating rate of 5°C/ min. The obtained powder agglomerates were manually milled and then calcined at 700°C for 2h (5°C/min) to promote the formation of the perovskite structure of PZT. After this second heat treatment, the carbon compounds were eliminated leading to nano-sized PZT powders with high purity. The columbic synthetic route employ is shown schematically in Fig. 1. Nano-sized PZT powders obtained were plasticized by 4 wt.% polyvinyl alcohol (PVA) addition, granulated and cold-pressed to disc-pellets at 120 MPa. Green ceramic discs (diameter (D): 10mm & thickness (t): 4.5 mm) were sintered (5°C/min) in $PbZrO_3$ rich atmosphere, at various temperatures.

Characterization

Density (ρ) of sintered discs was measured by the liquid displacement technique based on the Archimedes' principle. Silver paste was applied on both sides of ceramic discs as electrodes to provide a better ohmic contact for electrical measurements. Polarization was done at 120 °C/30 min in a silicon oil bath under a DC electric field of 15 kV/cm. The piezoelectric strain coefficient (d_{33}) of each disc was measured 24 h after poling, by a quasi-static d_{33} -meter (RM3500, KCF Tech). Coupling factor (k_p) and mechanical quality factor (Q_m) were determined by the resonance/ anti-resonance method using an Agilent 4294A impedance analyzer (*hp* Hewlett Packard). The parameters k_p and Q_m were related to the resonance frequencies by means of the following expressions [14,29,30]:

$$k_p = \left[\frac{f_a - f_r}{0.395 f_r + 0.574 (f_a - f_r)} \right]^{1/2}$$

$$Q_m = \frac{f_a^{\,2}}{2\pi Z_m C f_r \left(f_a^{\,2} - f_r^{\,2} \right)}$$

where f_r is the resonant frequency and f_a is the anti-resonant frequency in the fundamental vibration mode. Z_m and C represent the resonant impedance and the capacitance on the mechanical branch of the equivalent circuit, respectively.

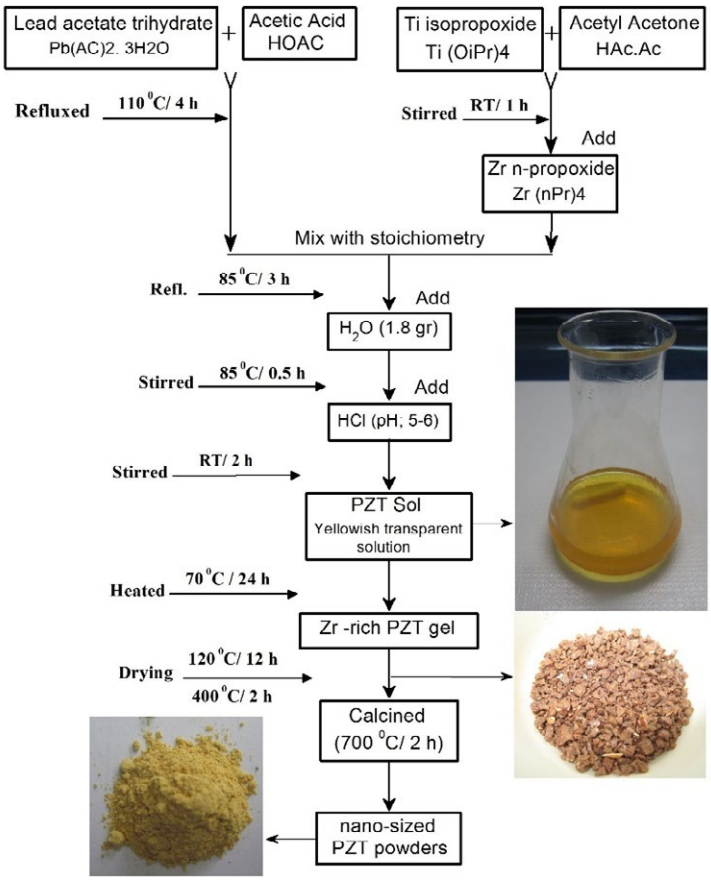

Fig. 1. Flow chart of PZT nanopowders synthesized.

Apparatus

Thermo-gravimetric analysis (TGA) and differential thermal analysis (DTA) with a heating rate of 5 °C/min was done to follow the phase evolution during heat treatment in air. Additionally, the phase purity and crystalline size were determined by an X-ray diffraction (XRD, D8-Advance Brucker diffractometer) with Cu kα radiation (λ=1.5418 °A), scanned 2θ from 20° to 85°). Energy dispersive X-ray spectroscopy (EDS) attaching to SEM was used to analyze the elemental composition. Particle size and morphological characteristics of PZT nanoparticles were monitored via scanning electron microscope (SEM; VEGATESCAN/LMU) and transmission electron microscope (TEM; Philips CM 30) at an accelerating voltage of 100 kV. The fine powder was dispersed onto a carbon coated copper grid. The electro-mechanical properties_ including; voltage constant (g_{33}), mechanical quality (Q_m) and coupling (k_p) factors, dielectric constant (ε), etc._ were examined using an Agilent 4294A impedance analyzer (hp Hewlett Packard) and the piezoelectric constant d_{33} was measured with a quasi-static d_{33} –meter (RM3500, KCF Tech.).

RESULT AND DISCUSSION

DTA-TG

Thermal decomposition behavior of PZT gel was examined by thermo gravimetry (TG) and differential thermal analysis (DTA), shown in Fig. 2. At temperature of up to 400 °C, endothermic (Ed) and exothermic (Ex) reactions may be attributed to the volatilization and burnout of residual solvent in the sol [5]. The Ed_1 peak at around 70 °C is due to the evaporation of water absorbed in the PZT solution (rate of weight loss: 4.173%). Also, the vaporization of light molecular organics occurs between 210-310 °C which corresponds to Ed_2, accompanied by a 27.492% weight loss. As a result, the exothermic peaks at 390, 480 and 530 °C were considered to be related to progressive decomposition of an organic group from Pb-Zr-Ti alkoxide and due to crystallization of metal

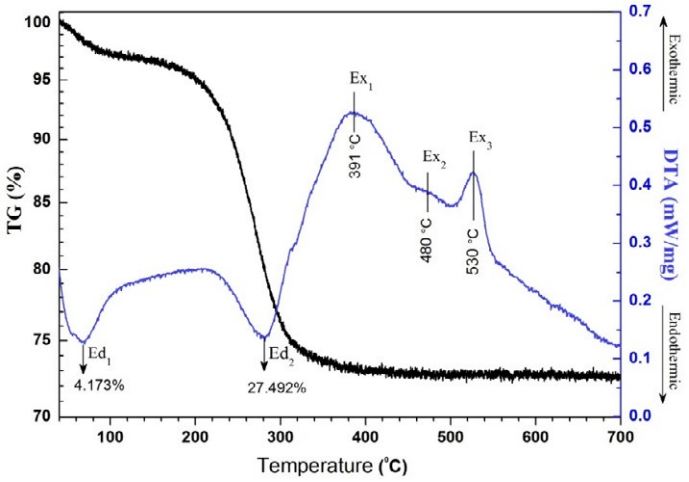

Fig. 2. TG/DTA curves of PZT gel powders.

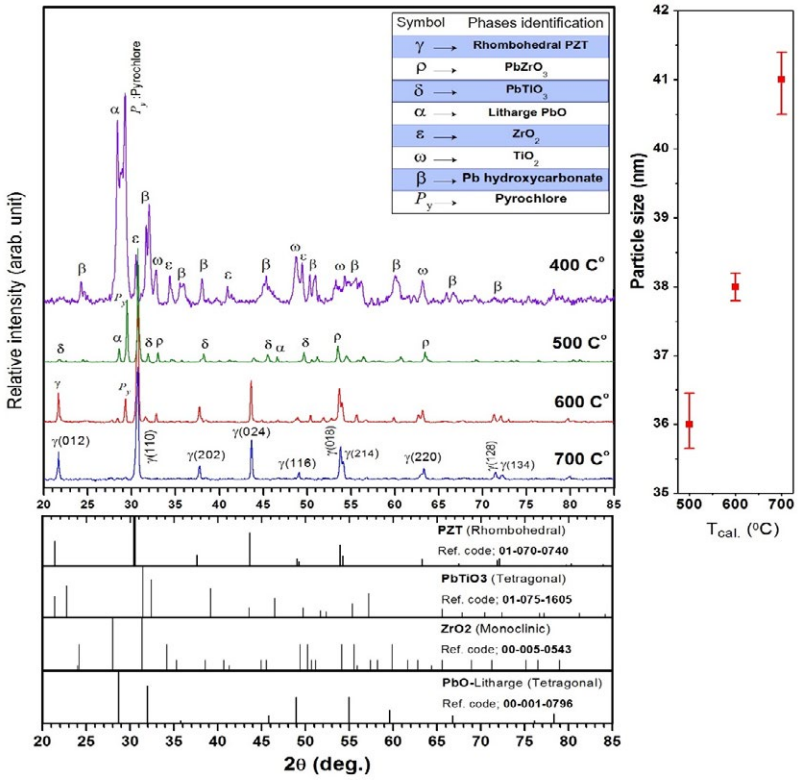

Fig. 3. XRD images of PZT nanopowders calcined at various temperatures.

oxide phase [3,5]. Therefore, crystallization of PZT powders takes place at 480 ˚C, and perovskite structure is established above 530 ˚C.

XRD

X-ray diffraction patterns of PZT nano-powders calcined at various temperatures are shown in Fig. 3. A series of characteristic peaks: (012), (110), (202), (024) and (018) crystal planes at 2θ values are observed of nanopowders, which can be indexed based on rhombohedral phase (ICDD No. 1-070-0740). The perovskite -type structure emerged at a higher temperature of 400 °C which is due to large grain size and high extent of crystallinity [2-5]. The

relative intensity of pyrochlore peak (29.4°) at calcination temperature of 400 °C with respect to PZT peak (30.62°) is much stronger. At temperature of 500 and 600 °C, the pyrochlore and perovskite phases coexisted, which is consistent with the results reported elsewhere [2,3,12]. However, the pyrochlore phase at 29.4° of 2θ was transformed into perovskite phases at temperatures of 700 °C. By comparison, it can be found from Fig. 3; (i) At 400 °C the powders calcined were already crystalline, and composed of phases of cerussite ($PbCO_3$: Ref. code 5-417), hydrocerussite ($Pb_3(CO_3)_2(OH)_2$: Ref. code 13-131), and laurionite (PbClOH: Ref. code 31-680), monoclinic zirconia (ZrO_2: Ref. code 5-543), and anatase titanium oxide (TiO_2: Ref. code 2-387). (ii) Following calcination at 500- 600 °C, the PZT precursors were composed of phases of litharge (PbO: Ref. code 1-796), $PbZrO_3$ (Ref. code 1-75-1607) and $PbTiO_3$ (Ref. code 1-75-1605). Lead hydroxyl carbonate phases (i.e., cerussite and hydrocerussite) were mostly converted into their oxides (i.e., litharge). (iii) Upon calcination at 700°C, the phases of litharge and pyrochlore completely disappeared, and the initial formation of rhombohedral PZT (Ref. code. ICDD 1-70-740) was observed. The average particle size (S_p) was calculated by the Debye– Scherrer formula [17]; $S_p = 0.89\lambda/\beta Cos\theta$, where λ is the X-ray wavelength (1.54 ˚A), θ the diffraction angle and β is the peak width of half maximum (the S_p of PZT nano-powders calcined at various temperatures are shown in Fig. 3.).

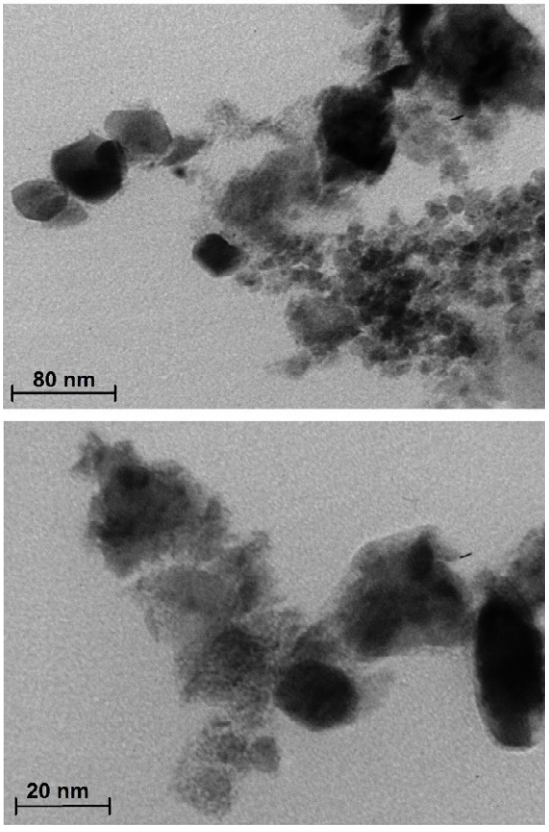

Fig. 4. TEM images of PZT nano-powders calcined at 700 °C.

SEM-TEM

Typical TEM micrographs of represent PZT nano-powders calcined at 700 °C are shown in Fig. 4. From Fig. 4, nearly spherical shape particles, highly crystalline nature and size distribution less than 20nm can be observed which is a relatively agglomeration state due to high surface energy of particles in nano-scale.

The surface morphology of PZT nano-powders nanocrystals was analyzed by scanning electron microscopy. Fig. 5 present the SEM photographs of PZT nano-powders calcined at 700 °C. Though the SEM images did not show well dispersed PZT nano-powders, but the PZT aggregated particles appear to be composed of much smaller crystallites. Also, to better identification of elemental composition of the synthesized material, Energy dispersive X-ray measurements were carried out by the EDX spectrometer attached to SEM. The EDS pattern of PZT is shown in Fig. 5f, which confirms the existence of Pb, Zr and Ti elements.

Piezoelectric study

To determine piezoelectric property of ceramics, resonant vibration spectrum of samples was measured at room temperature. Fig. 6 shows the impedance-phase spectra on frequency for piezo-ceramics sintered at 1150 °C. From these results, the resonant (f_r) and anti-resonant (f_a) frequencies, the minimum impedance Z_{min}, electromechanical coefficients K_p, mechanical quality factor Q_m and dielectric loss tanδ are defined and the value are listed in Table 1.

The variation of ceramic density as a function of sintering temperatures (T_{sint}: 1000-1250 °C) is shown in Fig. 7. A relative density of 7.53 g/cm^3 was achieved at sintering temperature of 1150 °C, which is close to the theoretical density (~95%). At higher T_{sint}, the density of ceramic samples strongly decreases which can be attributed to the evaporation of excess PbO.

The electromechanical properties of PZT ceramics as a function of sintering temperatures

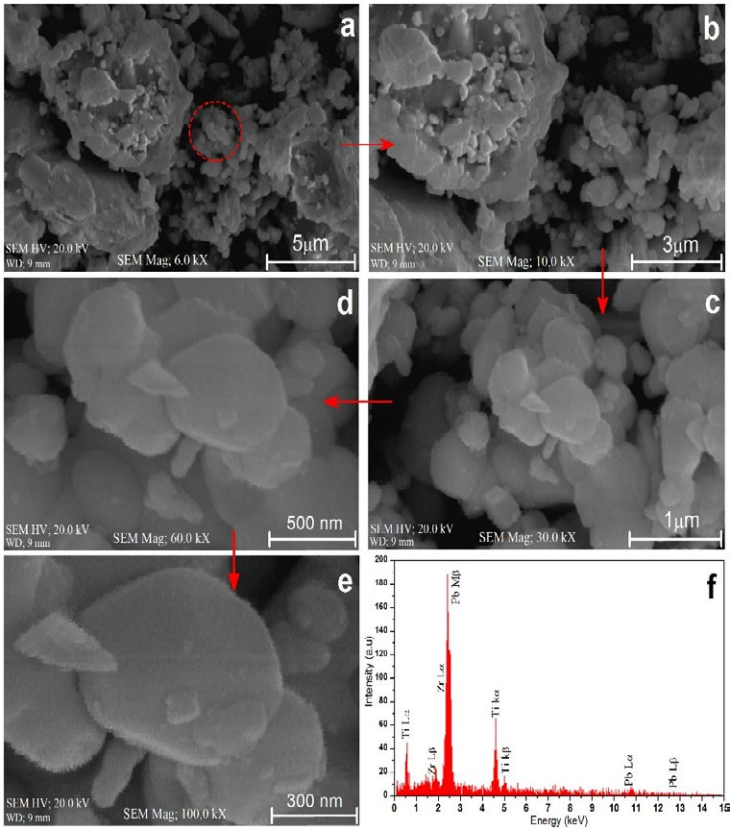

Fig. 5. SEM images of PZT nano-powders calcined at 700 °C.

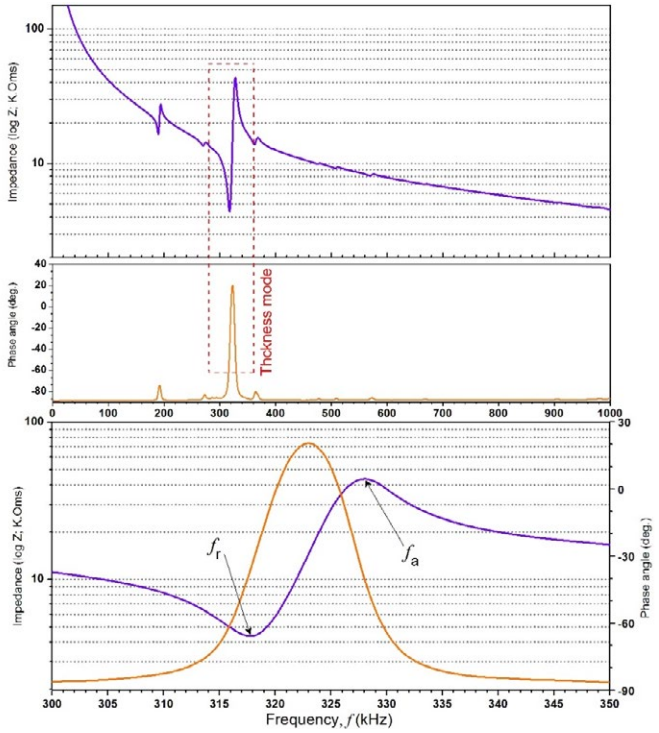

Fig. 6. The frequency spectra of piezo-ceramic sintered at 1150 °C.

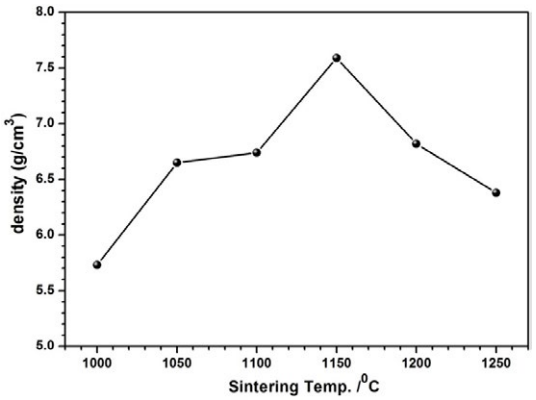

Fig. 7. The variation of ceramic density at sintering tempera tures.

are shown in Fig. 8. Both d_{33} and Q_m show a similar variation trend with increasing temperatures. The optimized values of d_{33} (64 pC/N) and Q_m (34.3 pC/N) were obtained 1150 °C. The K_p value of piezo-ceramics initially increases with increasing $T_{sint.}$ until it reaches a maximum value of 0.41 at 1150 °C, and then decreases for high temperature, which may be due to the evaporations of lead oxide. In addition, with decreasing $T_{sint.}$, dielectric constant (ε_r) increased continuously. This phenomenon is common for polycrystalline ferroelectric ceramics. In the past decades, effect of grain size on the relative permittivity has been extensively reported and different theoretical models have been introduced to describe the physical origin of this effect [27]. For example; in $BaTiO_3$, it is now widely accepted that ε_r increases with decreasing grain size, reaching a value of 5000, or higher, as the grain size approaches

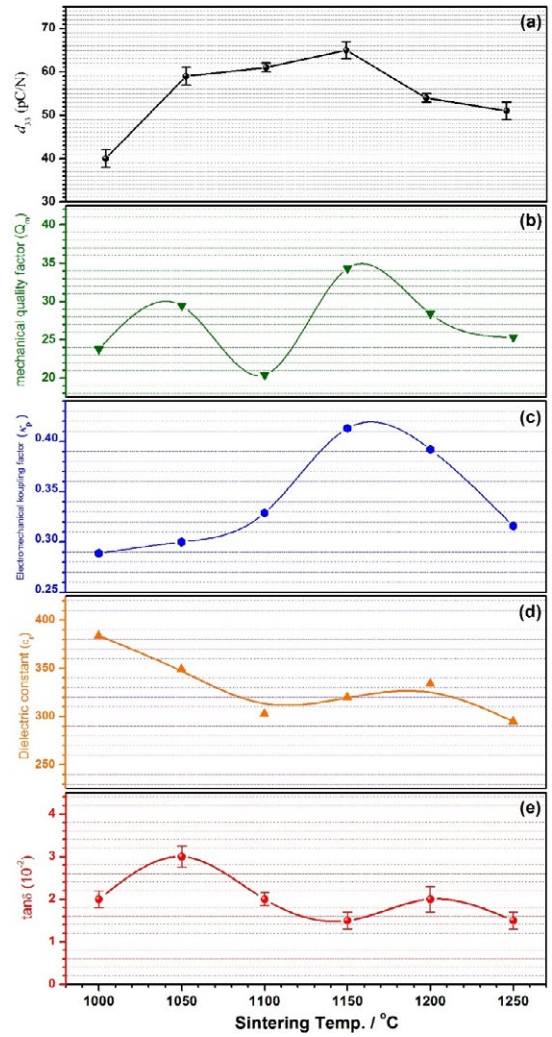

Fig. 8. The variation of (a) d_{33} (b) Q_m (c) K_p (d) ε_r and (e) tanδ as a function of sintering temperatures.

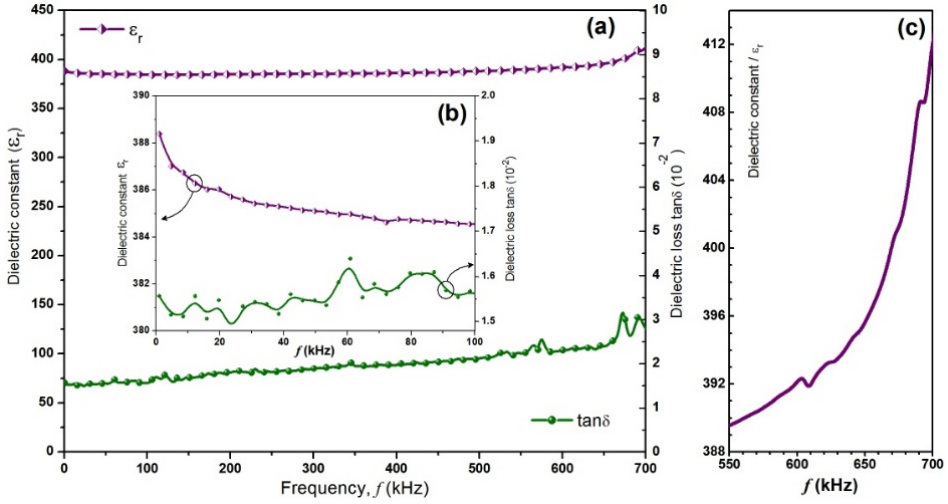

Fig. 9. The variation of dielectric constant (ε_r) and loss factor (tanδ) versus frequency.

Table 1. Piezoelectric properties of ceramic samples sintered at various temperatures.

	Sintering Temperature (°C)					
	1000	1050	1100	1150	1200	1250
Density (g/cm^3)	6.25	6.44	6.85	7.53	6.62	5.87
d_{33} (pC/N)	54	63	67	64	57	40
ε_r	384	349	303	320	334	295
Tgδ (%)	2	3	2	1.5	2	1.5
K_p	0.28	0.3	0.32	0.41	0.39	0.31
Q_m	23.7	29.4	20.4	34.3	28.4	25.3

1µm. Below 1µm, however, ε_r of $BaTiO_3$ decreases markedly with further decreasing grain size [28]. In our work, the maximum value (384) of ε_r was obtained for specimen with mean grain size of 1.84 µm sintered at 1000 °C. Further lowering the sintering temperature to obtain smaller grain size is impossible, because the sample is difficult to be densified.

Fig. 9a demonstrates the variations of the dielectric properties, *i.e.*, dielectric constant (ε_r) and loss tangent (tanδ) as a function of frequency. It can be seen for piezo-ceramic sintered at 1150 °C that both ε_r and tanδ are nearly independent of frequency and measured about 388 and 1.5% at 1 kHz, respectively. The dielectric constants decrease slowly at low frequency regime (Fig. 9b; ε_r < 390), which is may be attributed to the dielectric relaxation of PZT nanoparticles. Besides, the dielectric constants climb markedly with increasing frequency beyond 550 kHz (Fig. 9c). Dielectric relaxation of the ferroelectric ceramics could originate from the alternations of the elastic and electric behavior and the movement of the domain walls at high frequency regions [29].

CONCLUSION

The PZT nanopowders were synthesized by the sol-gel method using acetic acid as a complexing reagent. The PZT nanopowders with spherical-shaped morphology, perovskite structure and an average size of 20 nm are synthesized. The single PZT phase starts to form at a calcination temperature of 500 °C. The optimum piezoelectric parameters are obtained at sintering temperature 1150 °C: d_{33}=64 pC/N, K_p=0.41 and Q_m=34.3.

CONFLICT OF INTEREST

The authors declare that there are no conflicts of interest regarding the publication of this manuscript.

REFERENCES

1. Haertling GH. Ferroelectric Ceramics: History and Technology. Journal of the American Ceramic Society. 1999;82(4):797-818.
2. Whatmore RW. Pyroelectric Arrays: Ceramics and Thin Films. Journal of Electroceramics. 2004;13(1-3):139-47.
3. Noheda B. Structure and high-piezoelectricity in lead oxide solid solutions. Current Opinion in Solid State and Materials Science. 2002;6(1):27-34.
4. Guo R, Cross LE, Park SE, Noheda B, Cox DE, Shirane G. Origin of the High Piezoelectric Response inPbZr1−xTixO3. Physical Review Letters. 2000;84(23):5423-6.
5. Sakamoto WK, Marin-Franch P, Das-Gupta DK. Characterization and application of PZT/PU and graphite doped PZT/PU composite. Sensors and Actuators A: Physical. 2002;100(2-3):165-74.
6. Hsueh C-H, Wu C-C. Fabrication of lead zirconium titanium and silica composite films on copper/polyimide flexible substrates. Smart Materials and Structures. 2010;19(12):124005.
7. Jeff Duce, Scott Johnston, I.Y. Shen, G.Z. Cao, Hsien-Lin Huang, Method and sys-tem of fabricating PZT nanoparticle ink based piezoelectric sensor, in: UnitedStates Patent No. 8,614,724, 2013.
8. Kim SY, Tanimoto T, Uchino K, Nam CH, Nam S, Lee WI. Effects of PZT particle-enhanced ply interfaces on the vibration damping behavior of CFRP composites. Composites Part A: Applied Science and Manufacturing. 2011;42(10):1477-82.
9. Tanase T, Kobayashi Y, Konno M. Preparation of lead zirconate titanate thin films with a combination of self-assembly and spin-coating techniques. Thin Solid Films. 2004;457(2):264-9.
10. Ronald Staut, Brain Julius, John Meiman, PZT Powder Manufacturing, 2010,<www.ceramicindustry.com>.
11. Su B, Button TW, Ponton CB. Control of the particle size and morphology of hydrothermally synthesised lead zirconate titanate powders. Journal of Materials Science. 2004;39(21):6439-47.
12. Deng Y, Liu L, Cheng Y, Nan C-W, Zhao S-j. Hydrothermal synthesis and characterization of nanocrystalline PZT powders. Materials Letters. 2003;57(11):1675-8.
13. Wang SF, Wang YR, Mahalingam T, Chu JP, Lin KU. Characterization of hydrothermally synthesized lead zirconate titanate (PZT) ceramics. Materials Chemistry and Physics. 2004;87(1):53-8.
14. Harada S, Dunn S. Low temperature hydrothermal routes to various PZT stoichiometries. Journal of Electroceramics. 2007;20(2):65-71.
15. Traianidis M, Courtois C, Leriche A, Thierry B. Hydrothermal synthesis of lead zirconium titanate (PZT) powders and their characteristics. Journal of the European Ceramic Society. 1999;19(6-7):1023-6.
16. Chien AT, Sachleben J, Kim JH, Speck JS, Lange FF. Synthesis and characterization of PbTiO3 powders and heteroepitaxial thin films by hydrothermal synthesis. Journal of Materials Research. 1999;14(8):3303-11.

17. Deng Y, Liu L, Cheng Y, Nan C-W, Zhao S-j. Hydrothermal synthesis and characterization of nanocrystalline PZT powders. Materials Letters. 2003;57(11):1675-8.
18. Xu ZJ, Chu RQ, Li GR, Shao X, Yin QR. Preparation of PZT powders and ceramics via a hybrid method of sol–gel and ultrasonic atomization. Materials Science and Engineering: B. 2005;117(2):113-8.
19. Jayasinghe SN, Dorey RA, Edirisinghe MJ, Luklinska ZB. Preparation of lead zirconate titanate nano-powder by electrohydrodynamic atomization. Applied Physics A. 2005;80(4):723-5.
20. Lee S, Jun B. Preparation of ultrafine PZT powders by ultrasonic spray combustion synthesis (USCS). Ceramics International. 2005;31(1):53-6.
21. Chen YF, Nass R, Vilminot S. Seeding effects in the sol-gel preparation of lead zirconate titanate (PZT) powders. Journal of Sol-Gel Science and Technology. 1997;8(1-3):385-9.
22. Stefanescu M, Stoia M, Stefanescu O. Thermal and FT-IR study of the hybrid ethylene-glycol–silica matrix. Journal of Sol-Gel Science and Technology. 2006;41(1):71-8.
23. Faheem Y, Shoaib M. Sol-Gel Processing and Characterization of Phase-Pure Lead Zirconate Titanate Nano-Powders. Progress in Nanotechnology: John Wiley & Sons, Inc.; 2014. p. 147-50.
24. Qiu J, Tani J, Kobayashi Y, Um TY, Takahashi H. Fabrication of piezoelectric ceramic fibers by extrusion of Pb(Zr, Ti) O3powder and Pb(Zr, Ti)O3sol mixture. Smart Materials and Structures. 2003;12(3):331-7.
25. Yi G, Wu Z, Sayer M (1988) Preparation of Pb(Zr, Ti)O3 thin films by sol–gel processing. J Appl Phys 64(5):2717–2724.
26. Assink RA, Schwartz RW. Proton and carbon-13 NMR investigations of lead zirconate titanate (Pb(Zr,Ti)O3) thin-film precursor solutions. Chemistry of Materials. 1993;5(4):511-7.
27. M. Buscaglia, M. Viviani, V. Buscaglia, L. Mitoseriu, A. Testino, P. Nanni, Z. Zhao, M. Nygren, C. Harnagea, D. Piazza, C. Galassi, Phys. Rev. B 73 (2006).
28. D. Ghosh, A. Sakata, J. Carter, P.A. Thomas, H. Han, J.C. Nino, J.L. Jones, Adv. Funct. Mater. 24 (2014) 885–896.
29. J.E. Garcia, R. Perez, A. Albareda, J. Phys. D: Appl. Phys. 34 (2001) 3279.